Available online at www.sciencedirect.com
SCIENCE DIRECT
Scripta Materialia 54 (2006) 1363–1368
Scripta MATERIALIA
www.actamat-journals.com

A TEM study on TiB_2–20%$MoSi_2$ composite: Microstructure development and densification mechanism

Krishanu Biswas [a], Bikramjit Basu [b,*], Ashok Kumar Suri [c], Kamanio Chattopadhyay [a]

[a] Department of Metallurgy, Indian Institute of Science, Bangalore, India
[b] Department of Materials and Metallurgical Engineering, Indian Institute of Technology, Kanpur, UP 208 016, India
[c] Materials Group, Bhabha Atomic Research Center, BARC, Mumbai, India

Received 29 August 2005; received in revised form 28 November 2005; accepted 1 December 2005
Available online 18 January 2006

Abstract

We report the results of transmission electron microscopy (TEM) study, carried out on a hot-pressed TiB_2–20 wt.%$MoSi_2$ composite. One of the important microstructural observations includes the detection of crystalline $TiSi_2$ at triple grain junctions. The densification mechanism is discussed, based on experimental observations and thermodynamic analysis.

Keywords: TiB_2; $MoSi_2$; Hot pressing; TEM

1. Introduction

Non-oxide ceramics, in particular TiB_2, are candidate materials for high temperature structural applications due to their attractive properties like high melting point, superior thermal and electrical conductivities, high elastic modulus, high hardness and good corrosion resistance [1]. Despite possessing useful properties, the engineering applications of monolithic TiB_2 are rather limited because of poor sinterability. To obtain dense borides, various metallic and non-metallic binders have been explored [2–6]. However, for high temperature applications, the use of ceramic sinter-additives is preferred. In recent times, we have been able to demonstrate that $MoSi_2$ addition improves the sinterability of TiB_2 and that dense TiB_2–20 wt.%$MoSi_2$ composite can be obtained through hot pressing at 1700 °C for 1 h [7]. Higher hardness of ~25–26 GPa along with moderate fracture toughness of 4–5 MPa $m^{1/2}$ is measured with TiB_2–20 wt.% $MoSi_2$ composites. These novel materials also exhibit better wear resistance properties than monolithic TiB_2 [8]. In the present work, we examine the microstructure development in TiB_2–$MoSi_2$ composites in order to gain an insight into the densification mechanism during hot pressing.

Transmission electron microscopy (TEM) is a powerful tool to explore microstructure at small length scale, essentially for revealing process mechanisms. Torizuka et al. [3,4], using the TEM technique, observed the formation of grain boundary liquid phase (amorphous SiO_2) when SiC is used as an additive to TiB_2. Moreover, they identified the presence of a liquid phase $(Ti,Zr)_5Si_3$ at triple points in TiB_2–19.5 wt.%ZrO_2–2.5/5.0 wt.%SiC composite processed via the hot isostatic pressing route. Li et al. [5] identified the formation of BN, TiN, Al_2O_3 phases in TiB_2–20 wt.%AlN composite fabricated by hot pressing at 1800 °C. In another work, Park et al. [6] reported the formation of different reaction products like TiN and BN in TiB_2–2.5–10 wt.%Si_3N_4 composites (sintered at 1800 °C) and observed that Si_3N_4 acts as a grain growth inhibitor.

A critical literature analysis reveals that neither any detailed TEM work, nor any report on densification mechanism is available for TiB_2–$MoSi_2$ composites. In view of its excellent mechanical and tribological properties, further study has been conducted to characterize in detail the

* Corresponding author. Tel.: +91 512 2597771; fax: +91 512 2597505.
E-mail address: bikram@iitk.ac.in (B. Basu).

1359-6462/$ - see front matter
doi:10.1016/j.scriptamat.2005.12.001

microstructure evolution in TiB_2–$MoSi_2$ composites. Additionally, in order to further optimize the sintering aid content and sintering parameters, it is necessary to understand the mechanisms of sintering through a detailed analysis of the microstructure. The present contribution aims to meet this goal.

2. Experimental

The in-house processed TiB_2 and $MoSi_2$ powders were selected as starting powders for composite production. TiB_2 powder had been obtained by borothermic reaction between TiO_2 (Merck, Germany), B_4C (in-house processed) and carbon (99% purity, M/S Assam Carbon, India). B_4C powders were processed using carbothermic reduction of boric acid (HBO_3). The major impurities of as synthesized TiB_2 include oxygen (0.5 wt.%) and carbon (0.6 wt.%), as determined by the vacuum fusion analysis technique (Leco Industries, USA). The TiB_2 powders have an average particle size around 1.1 μm (ASTM standard, D_{50}). $MoSi_2$ was synthesized from elemental powders of Mo (>99% purity, supplier Leco Industries, USA) and Si (>99% purity, supplier Merck, Germany). Mechanical grinding was employed to reduce the size of the $MoSi_2$ powder after synthesis to yield finer particle size with D_{50} (mean particle diameter) around 1.4 μm.

Appropriate amount of powders with TiB_2:$MoSi_2$ in 80:20 (wt.%) ratio were mixed using a WC grinder. The densification was performed by hot pressing under vacuum (10^{-5} Pa) and 32 MPa pressure, using a 10 mm diameter graphite die. The samples were hot-pressed at 1700 °C for 1 h. A heating rate of 15 °C/min was used to achieve the temperature. The crystalline phases in the starting powders and hot pressed samples were analyzed using powder X-ray diffraction (XRD) (Rich-Seifert 2000D). The detailed microstructural analysis was performed using a scanning electron microscope (SEM, FEI model SIRION), operated at 20 kV and TEM (JEOL 2000 FXII) operated at 200 kV. Compositional measurements on the flat polished sections of the hot pressed composites were performed using an energy dispersive spectroscopy (EDS) detector (ultrathin window, capable of detecting boron), attached to a SIRION FEG-SEM. The volume fraction of various ceramic phases was calculated using SigmaScan Pro image processing software (Version 4, Jandel Scientific, USA). Thin foil for TEM was prepared following standard ion beam thinning procedure.

3. Results

XRD patterns acquired from the hot-pressed composite as well as from the starting powders are shown in Fig. 1. XRD results indicate the predominant presence of TiB_2, $MoSi_2$ and a small amount of $TiSi_2$ in the composite. The formation of $TiSi_2$ originates from sintering reaction, which will be discussed in detail later. No sign of TiO_2 or SiO_2 is observed within the detection limit of XRD.

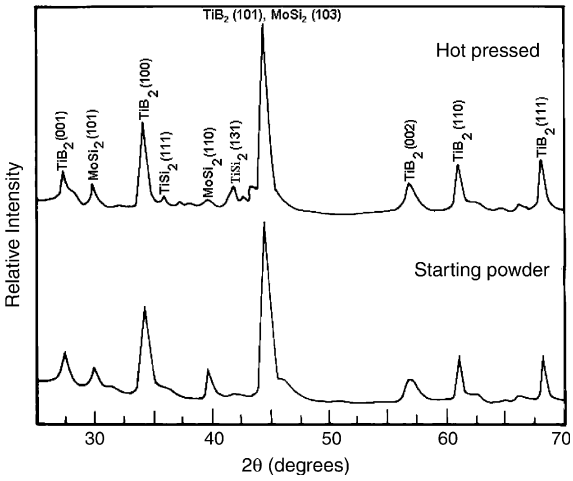

Fig. 1. XRD spectra showing the phase analysis of the starting powder and hot-pressed TiB_2–20 wt.%$MoSi_2$. The different crystalline phases are also indexed.

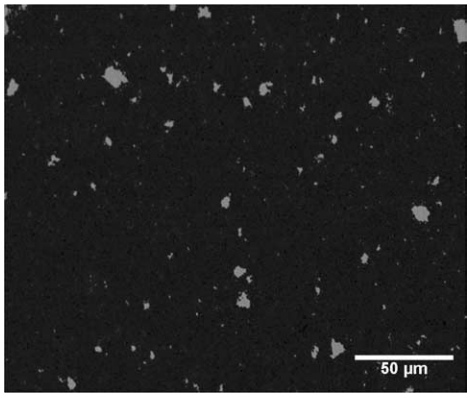

Fig. 2. Representative low magnification back scattered SEM image, showing distribution of $MoSi_2$ (bright contrast) in TiB_2 matrix.

Fig. 2 is a back scattered scanning electron (BSE) micrograph showing the distribution of the TiB_2 and $MoSi_2$. One can note the distribution of $MoSi_2$ (5 μm or coarser) which appears in brighter contrast in the TiB_2 matrix. As will be evident from the TEM observations, described later, the observed $MoSi_2$ phase on SEM image is in fact agglomerates of finer $MoSi_2$ particulates. From low magnification BSE images, the volume fractions of the $MoSi_2$ and TiB_2 were calculated using commercial image analysis software (SigmaScan Pro image processing, version 4, Jandel Scientific, USA). The average volume fractions of the two phases, as calculated by random sampling, were: $MoSi_2 = 16\%$ and $TiB_2 = 84\%$. Using the known density of these two phases (densities of $MoSi_2 = 5.57$ gm/cc and $TiB_2 = 4.52$ gm/cc), the amount (in wt.%) of $MoSi_2$ was found to be 19.1%, which is consistent with the compositional analysis using EDS.

A detailed microstructural characterization of the sintered TiB_2–20% $MoSi_2$ samples was carried out using TEM. Fig. 3a and b are bright field and dark field pair from a typical grain. Selected area diffraction pattern

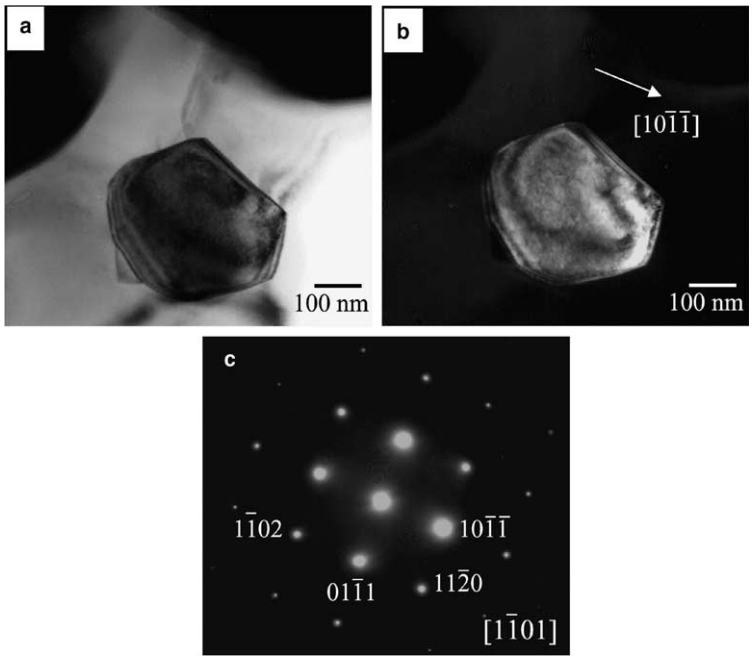

Fig. 3. (a) Bright field TEM image showing faceted equiaxed grain morphology of TiB_2 particles in hot-pressed composite, (b) dark field image of the same TiB_2 particle showing no evidence of defect structure and (c) corresponding SAD pattern.

(SADP) analysis from the same grain is shown in Fig. 3c. The diffraction analysis confirms these to be TiB_2 with a hexagonal close-packed (hcp) structure. It may be noted that the room temperature lattice parameters of hcp TiB_2 are: $a = 0.303$ nm and $c = 0.3229$ nm. The grain size of TiB_2 varies between 1 and 1.2 μm. The dark field image (Fig. 3b) shows a clean grain in the present case and the absence of dislocations. The absence of any defect substructure was noticed in most of the investigated TiB_2 grains.

Fig. 4 presents the morphology of a $MoSi_2$ grain, as recorded under different imaging conditions. The bright field image (Fig. 4a) reveals an elongated $MoSi_2$ grain with a few faceted grain boundaries. The strong beam dark field image using (0 0 1) reflection is shown in Fig. 4c. The grain size of $MoSi_2$ particles (as measured using dark field

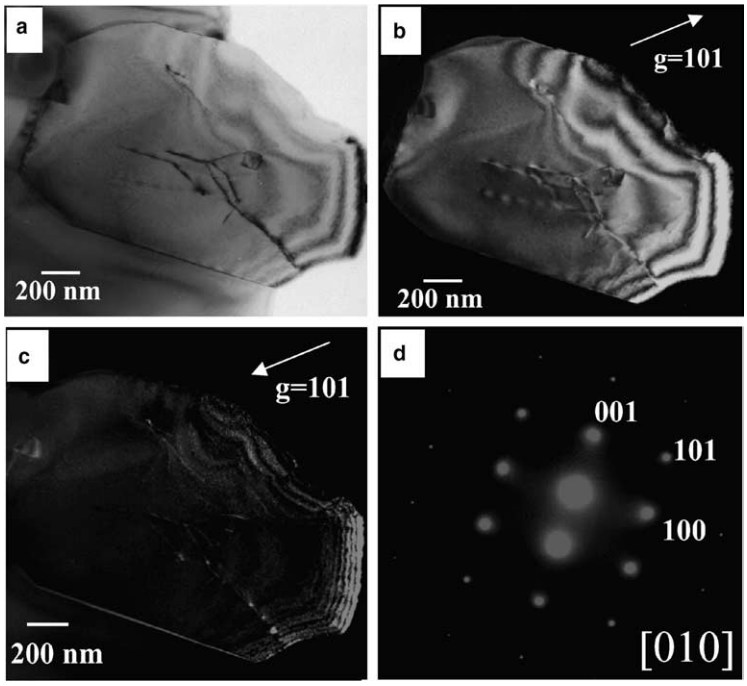

Fig. 4. (a) Bright field TEM image of a $MoSi_2$ grain showing dislocation activity, (b) strong beam, (c) weak beam dark field images showing dislocations and (d) SAD pattern from $MoSi_2$ grain.

images) varies between 1.2 and 2 μm and the typical aspect ratio of elongated $MoSi_2$ particles is about 4. The SADP pattern (Fig. 4d), obtained with beam orientation along one of the mutually orthogonal zone axis [0 1 0], confirms the tetragonal structure of $MoSi_2$. The crystal structure analysis indicates that the lattice parameters (at room temperature) of $MoSi_2$ are: $a = 0.3204$ nm and $c = 0.7844$ nm.

Considering the initial particle sizes of TiB_2 ($D_{50} \sim 1.1$ μm) and $MoSi_2$ ($D_{50} \sim 1.4$ μm), the above observation indicates that hot pressing at 1700 °C did not promote any significant grain growth. In an earlier study, Torizuka et al. [3] had observed extensive grain growth when 20 wt.%ZrO_2 was used as a sintering additive to densify TiB_2 at 1700 °C. The present observation is in contrast to this result and indicates that $MoSi_2$ could potentially act as a grain growth inhibitor for TiB_2.

The defect sub-structure, i.e. the presence of dislocation, is clearly visible in the $MoSi_2$ grains. Weak beam dark field imaging was used for the observation of the defect structure (Fig. 4c). The presence of dislocations in the central region of $MoSi_2$ grain is clearer under the weak beam condition. Dislocation activity could be seen in all the $MoSi_2$ grains. In some cases, the presence of dislocation tangles (not shown) is observed within $MoSi_2$ grains. This type of dislocation tangle was observed earlier [9] in $MoSi_2$–1 at.%Nb alloy, compressed at 1600 °C. Dislocation cell-structures, i.e. subgrain formation, was also reported [10] earlier in $MoSi_2$ monoliths following compressive deformation at temperatures above 1300 °C.

The detailed TEM observations of the phase at a grain boundary triple point are presented in Figs. 5 and 6. Fig. 5 shows two different grain configurations in which

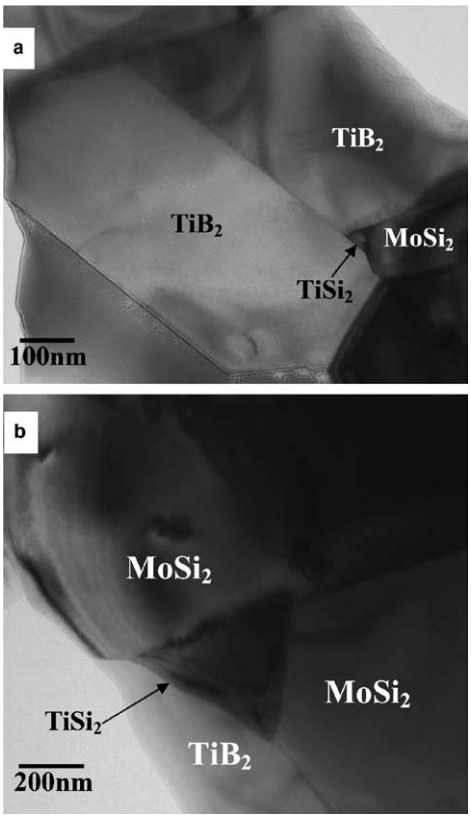

Fig. 5. Bright field TEM images revealing the formation of $TiSi_2$ at the triple grain junction point in two different situations: (a) $TiSi_2$ is surrounded by two TiB_2 and one $MoSi_2$ grain; (b) $TiSi_2$ is surrounded by one TiB_2 and two $MoSi_2$ grain. The size of $TiSi_2$ is much smaller in the first case as compared to the second one.

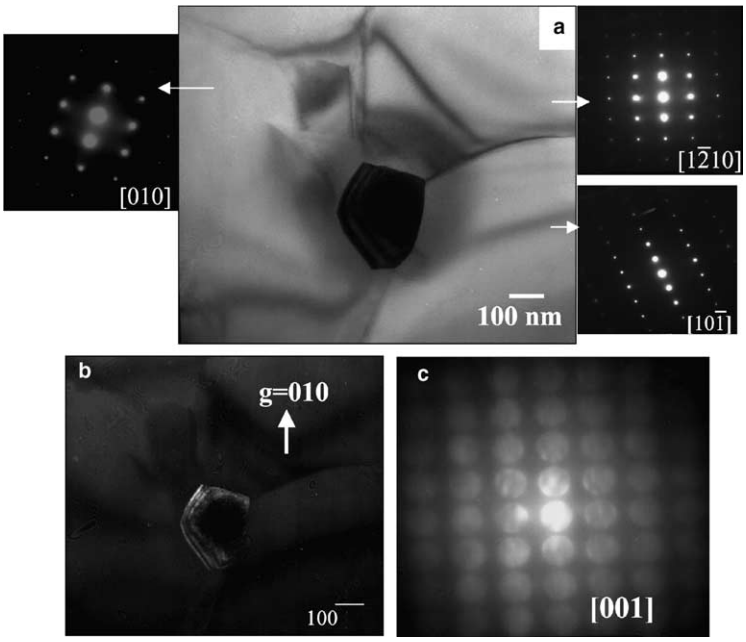

Fig. 6. (a) Bright field TEM image showing the a $TiSi_2$ particle at the triple grain junction point with insets showing SAD patterns taken from three surrounding grains; (b) dark field image of the $TiSi_2$ particle and (c) micro-diffraction pattern taken from the $TiSi_2$ grain.

$TiSi_2$ has been found to be formed at the triple junction point. Fig. 5a illustrates that $TiSi_2$ is surrounded by two TiB_2 and one $MoSi_2$ grains whereas Fig. 5b reveals that $TiSi_2$ is surrounded by two $MoSi_2$ grains and one TiB_2 grain. One can see that the size of the $TiSi_2$ is much smaller in the former case as compared to the second one. More importantly, the interfaces are either planar or curved with concaveness towards the $TiSi_2$ phase suggesting a wetting tendency of this phase. Fig. 6a shows a typical bright field image of a $TiSi_2$ grain surrounded by two TiB_2 grains and one $MoSi_2$ grain. The SAD pattern taken from the surrounding TiB_2 and $MoSi_2$ grains are shown as insets of Fig. 6a. The micro diffraction pattern obtained from the phase at the triple junction point along [0 0 1] is shown in Fig. 6c. The analysis of the recorded pattern confirms the presence of orthorhombic $TiSi_2$ phase at the triple junction ($a = 0.8268$ nm, $b = 0.8553$ nm and $c = 0.4798$ nm). Bright field TEM images reveal that the size of the crystalline phase at a triple pocket varies between 30 and 400 nm. The faceted crystalline morphology of this phase is clearer in the dark field image, presented in Fig. 6b.

4. Discussion

We will first summarize the important facts that have emerged from the present investigation as they are relevant for developing an understanding of the sintering process. Besides $MoSi_2$ and TiB_2, the sintered ceramic composite contains a small amount of $TiSi_2$. $TiSi_2$ has a melting point of 1500 °C (1773 K) and hence must be molten at the sintering temperature (1700 °C). TEM studies indicate that this phase exists at the triple points with at least one of the surrounding grains being $MoSi_2$. Thus, the microstructural observations strongly suggest that densification of TiB_2–$MoSi_2$ composite occurred by liquid phase sintering, involving rearrangement of grains by capillary action in the presence of wetting liquid phase $TiSi_2$. However, the reaction path leading to formation of $TiSi_2$ phase remains to be determined. Let us now discuss the possible ways $TiSi_2$ could be formed.

It is reported in the literature that surface layers of TiO_2 and B_2O_3 can exist on the surfaces of TiB_2 particles [12]. Literature report also indicates that B_2O_3 vaporizes rapidly above 1127 °C (1400 K) [12]. In our hot pressing experiment, 4–6% weight loss is measured and this is attributed to the evaporation of the volatile oxides (B_2O_3, MoO_3). In the presence of surface oxides, $TiSi_2$ can be formed by a reaction between TiO_2 and $MoSi_2$:

$$TiO_2 + MoSi_2 \rightarrow TiSi_2 + MoO_2(g) \quad (1)$$

Based on the available thermodynamic data of the energy of formation of different compounds, this reaction is not thermodynamically feasible at and below the sintering temperature of 1973 K (Fig. 7).

Although the experiments have been carried out inside a vacuum chamber (10^{-5} Pa), residual oxygen will be present during the hot pressing experiment. In the case where oxygen is present in the sintering environment, the following reaction is possible:

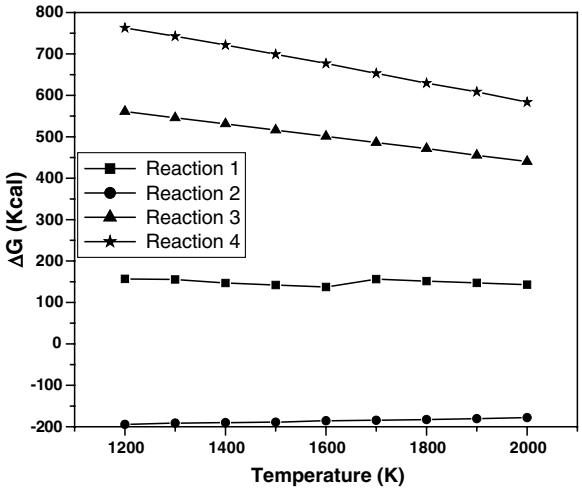

Fig. 7. Plot showing the Gibbs free energy change of the four reactions (1)–(4) as a function of temperature.

$$TiB_2 + 3O_2(g) + MoSi_2 \rightarrow TiSi_2 + B_2O_3(g) + MoO_3(g) \quad (2)$$

The overall free energy change for this reaction to proceed in the forward direction is negative at and below 1973 K. For example, ΔG at 1800 K is estimated to be −183.10 kcal. Hence this reaction leading to formation of $TiSi_2$ is thermodynamically feasible.

There exist other alternative possibilities for the formation of $TiSi_2$. It is reported that the $MoSi_2$ grains are often covered by a SiO_2 layer due to low temperature oxidation [11]. This layer co-exists with MoO_3, which vaporizes at higher temperatures [13]. The presence of SiO_2 at the interface between $MoSi_2$ and TiB_2 grains can promote the following possible sintering reactions:

$$MoSi_2 + 7TiB_2 + 12SiO_2 \rightarrow 7TiSi_2 + 7B_2O_3(g) + MoO_3(g) \quad (3)$$

$$5MoSi_2 + 14TiB_2 + 21SiO_2 \rightarrow Mo_5Si_3 + 14TiSi_2 + 14B_2O_3(g) \quad (4)$$

The free energy calculations for these two reactions indicate a positive free energy change for the reactions to proceed from left to right at the sintering temperature. However, these reactions may be feasible at temperatures higher than the hot pressing temperature. The fact that the presence of Mo_5Si_3 has neither been detected by XRD nor observed during the TEM investigation rules out the reaction (4) in the present case. It can be noted that Mo_5Si_3 phase is reported to form during high temperature oxidation of $MoSi_2$ [11]. The changes in Gibbs energy values as a function of temperature for all the above reactions are summarized in Fig. 7.

On the basis of the thermodynamic calculations, there is only one possibility for the formation of $TiSi_2$ phase at the

sintering temperature (1973 K). From Fig. 7, it is evident that the $TiSi_2$ phase forms and grows during the sintering primarily through reaction (2). The equilibrium partial pressure [14] of oxygen (p_{O_2}) required for reaction (2) is calculated to be 2.5×10^{-14} Torr, which is much lower than the p_{O_2} level of 2.7×10^{-5} Torr, estimated to be present in the hot press chamber during sintering. This estimation of p_{O_2} is done by considering a vacuum level of 10^{-5} Pa (see Section 2) to be present in the hot press chamber and assuming that the O_2:N_2 ratio in the vacuum is the same as that in ambient air. Therefore, the formation of $TiSi_2$ is highly likely even in the weak oxidizing condition that is present in the hot press chamber. At the sintering temperature, $TiSi_2$ is molten and aids the sintering process by wetting the grain boundaries enabling enhanced capillary driven mass transport. This process is also accompanied by grain rotations, necessary for densification.

The TEM analysis indicates the absence of any dislocation activity in TiB_2 and a significant presence of dislocations in $MoSi_2$ grains. The observation of finer TiB_2 grain sizes is also important. In the case of TiB_2, the anisotropic thermal contraction behavior is reported to the formation of microcracks during post-fabrication cooling in the case of grain size exceeding the critical grain size of 20 μm [7]. Thus, a finer TiB_2 starting powder as well as lower densification temperature, as employed in the present work, is useful to obtain finer grain size and crack free dense material. The presence of such finer TiB_2 grains also leads to the attainment of high hardness (25 GPa). However, the fracture toughness of these novel materials remains moderate and around 5 MPa $m^{1/2}$. Further investigation is under way to improve the toughness properties.

Another important result of the present study is the evidence for the presence of $TiSi_2$ at the grain boundary triple pocket. It is possible that $TiSi_2$ can form due to solid-state reaction between TiB_2 and $MoSi_2$ during heating of the powder compact at lower temperature by reaction (2). From a study of relevant binary and ternary phase diagrams of systems based on Mo,Ti and Si, [15] it is evident that $TiSi_2$, even if formed in solid-state, would melt (melting temperature: 1733–1753 K) and form a sintering liquid at the hot pressing temperature of 1973 K. TEM investigation further reveals that $TiSi_2$ is present only at the grain boundary triple pockets in the sintered microstructure. This has most likely occurred due to the migration of the liquid during sintering. The migration of all the $TiSi_2$ in the solid-state to the triple points is unlikely due to the limited diffusion in the solid-state. Therefore, we conclude that the densification mechanism is dominated by liquid phase sintering in the presence of a sintering liquid i.e. $TiSi_2$ phase ($T_m \sim 1773$ K).

5. Conclusions

Based on the present results and discussion, we can arrive at the following conclusions:

(a) The presence of $MoSi_2$ aids in the sintering of TiB_2–20 wt.%$MoSi_2$ composites through the formation of small amount of $TiSi_2$ phase, which is liquid at a hot pressing temperature of 1700 °C. The morphology of this phase at the triple points suggests that it can wet the TiB_2–$MoSi_2$ interface. The densification is assisted by liquid phase sintering.

(b) The hot-pressed microstructure is characterized by the presence of finer TiB_2 grains. None of the investigated boride grains show any observable dislocation activity. On the other hand, $MoSi_2$ particulates are coarser (>1 μm) and the presence of significant dislocation activity is critically noted.

(c) Thermodynamic analysis of the various possible reactions indicates that the most likely reaction pathway for the formation of $TiSi_2$ is

$$TiB_2 + 3O_2(g) + MoSi_2 \rightarrow TiSi_2 + B_2O_3(g) + MoO_3(g)$$

This reaction can take place at a partial pressure of oxygen as low as 2.5×10^{-14} Torr.

Acknowledgement

The financial support of the Board of Research in Nuclear Science (BRNS) programme of Department of Atomic Energy (DAE), Government of India is gratefully acknowledged.

References

[1] Cutler RA. Engineering properties of borides. In: Engineered materials hand book. Ceramics and glasses, vol. 4. Metals Park (OH): ASM International; 1991. p. 787.
[2] Jones AH, Debedoe RS, Lewis MH. J Am Ceram Soc 2001;21:969–80.
[3] Torizuka S, Sato K, Harada J, Yamamot H, Nishio H. J Ceram Soc Jpn 1992;100(4):392–7.
[4] Torizuka S, Sato K, Nishio H, Kishi T. J Am Ceram Soc 1995;78(6):1606–10.
[5] Li LH, Kim HE, Kang ES. J Eur Ceram Soc 2002;22:973–7.
[6] Park JH, Koh Y, Kim H, Hwang C, Kong E. J Am Ceram Soc 1999;82(11):3037–42.
[7] Murthy TSRCh, Basu B, Balasubramaniam R, Suri AK, Subramoniam C, Fotedar RK. J Am Ceram Soc 2006;89(1):131–8.
[8] Murthy TSRCh., Basu B, Srivastava A, Balasubramaniam R, Suri AK. J Eur Ceram Soc, in press.
[9] Ferber MK, Becher PF, Finch CB. Commun Am Ceram Soc Jan 1983:C-2–3.
[10] Sharif AA, Misra A, Mitchell TE. Mat Sci Eng A 2003;358:279–87.
[11] Kuchino J, Kurokawa K, Shibayama T, Takahashi H. Vacuum 2004;73:623–8.
[12] Baik S, Becher PF. J Am Ceram Soc 1987;70(8):527–30.
[13] Becker S, Rahmel A, Schütze M. Solid State Ionics 1992;53–56:280–9.
[14] Lupis CHP. Chemical thermodynamic of materials. Amsterdam: North-Holland; 1983.
[15] Murray JL. Ti–Si phase diagram. ASM Handbook. Alloy phase diagrams, vol. 3. Metals Park (OH): ASM International; 1992. p. 367.